© 2015 IEEE.Personal use of this material is permitted. Permission from IEEE must be obtained for all other uses, in any current or future media, including reprinting/republishing this material for advertising or promotional purposes,creating new collective works, for resale or redistribution to servers or lists, or reuse of any copyrighted component of this work in other works
doi: 10.1109/JPHOTOV.2015.2392945

Microscale Spatially Resolved Characterization of Highly Doped Regions in Laser-Fired Contacts for High-Efficiency Crystalline Si Solar Cells

A. Roigé, J. Alvarez, J.-P. Kleider, I. Martín, R. Alcubilla, and L. F. Vega

***Abstract*—Laser-fired contact (LFC) processes have emerged as a promising approach to create rear local electric contacts in p-type crystalline silicon solar cells. Despite this approach has been successfully applied in devices showing efficiencies above 20%, there is still a lack of knowledge about some specific features of LFCs at the submicron level. In this study, we used micro-Raman and microphotoluminescence (PL) spectroscopies to carry out a high-resolution spatially resolved characterization of LFCs processed in Al_2O_3-passivated c-Si wafers. Relevant information concerning features such as local doping distribution and crystalline fraction of the laser-processed region has been obtained. In particular, interesting qualitative and quantitative variations concerning the doping profile have been observed between LFCs processed at different laser powers. Finally, conductive-atomic force microscopy measurements have allowed to identify the existence of highly conductive zones inside the LFCs greatly correlated with highly doped regions revealed by Raman and PL data. This study gives a detailed insight about the LFCs characteristics at the submicron level and their possible influence on the performance of final devices.**

***Index Terms*—Crystalline silicon, laser-fired contacts (LFCs), microphotoluminescence spectroscopy, micro-Raman spectroscopy.**

I. Introduction

FROM an industrial point of view, one of the most interesting crystalline silicon (c-Si) solar cell technologies to obtain high-efficiency devices is the passivated emitter and rear cell concept. Recently, the industrial implementation of this cell type has been significantly simplified by using the so-called laser fired contact (LFC) approach for the creation of the back contacts of the cell [1], [2]. This method is based on firing the rear Al metallization layer by a laser beam in order to create electrical point contacts between the Al layer and the silicon substrate through the passivation layer.

A key feature for the good operation of LFCs is the formation of an Al-doped p+ region under the contacted surface area. This is achieved by the diffusion of Al atoms from the predeposited Al layer into the molten Si. This p+ region not only creates a local back-surface field that induces a relatively low recombination velocity below the contacts, but also ensures a low-contact resistance.

LFC approach can be applied by using any of the dielectric layers that have demonstrated excellent c-Si passivating properties such as silicon oxide (SiO_2) [3], silicon nitride (SiN_x) [4], amorphous-silicon carbide (a-SiC_x) [5], and most recently, aluminum oxide (Al_2O_3) [6]. In the case of using the latter passivating material, an interesting alternative to the conventional LFC process can be applied. In this case, the Al_2O_3 layer itself can be used as Al-dopant source for the formation of the p+ region, and hence, the LFC can be done directly onto the Al_2O_3/c-Si, instead of being done onto the Al/dielectric/c-Si stack. This approach enables a lower laser power operation in comparison with conventional LFC process where higher laser powers are needed to fire the aluminum through the dielectric layer. These type of LFC processes have been already used to fabricate solar cells showing efficiencies well above 20% [6].

Despite the evident success in the implementation of the LFC approach in real devices, there is still a lack of information about specific features of LFCs such as the doping profile of the p+ region, the level of induced-stress, and/or the structural properties of the laser-processed region. The most likely reason for that is the difficulty to find experimental techniques that match a high-lateral resolution (below 10 μm) and sensitivity to the parameters wanted to be studied. Recently, a study of LFC cross sections [7] have demonstrated that Raman and photoluminescence (PL) spectroscopies in microconfiguration are techniques that fulfill the mentioned requirements.

In this study, we have carried out high-resolution micro-Raman and micro-PL spectroscopy measurements on different LFCs processed in Al_2O_3-passivated c-Si samples. Thanks to the high lateral resolution down to 1 μm achieved in our experiments, we have been able to perform a detailed study of relevant LFC properties such as the doping profile, induced-stress, and crystallinity fraction, giving an important insight about the LFC formation. Three LFCs processed at different incident laser power have been studied in order to analyze the influence of the laser power on the studied features. Finally, in

Manuscript received October 29, 2014; revised December 20, 2014; accepted January 5, 2015. This work was supported by Carburos Metálicos/Air Products Group, the Generalitat of Catalonia (Project SGR2014-1582), and the Spanish Government (Project TEC2011-26329). This work was also supported in part by the project HERCULES that has received funding from the European Union's Seventh Programme for Research Technological Development and Demonstration under Grant Agreement 608498. The work of A. Roigé was supported through a TALENT fellowship from the Generalitat of Catalonia.

A. Roigé is with MATGAS Research Center, 08193 Bellaterra, Spain (e-mail: aroige@matgas.org).

J. Álvarez and J.-P. Kleider are with the LGEP-Supelec, 91192 Gif sur Yvette, France (e-mail: jose.alvarez@lgep.supelec.fr).

I. Martín and R. Alcubilla are with the Departament d'Enginyeria Electrònica, Universitat Politècnica de Catalunya, 08034 Barcelona, Spain (e-mail: isidro.martin@upc.edu; ramon.alcubilla@upc.edu).

L. F. Vega is with MATGAS Research Center, Carburos Metálicos-Air Products Group, 08009 Barcelona, Spain (e-mail: vegal@carburos.com).

Color versions of one or more of the figures in this paper are available online at http://ieeexplore.ieee.org.

Digital Object Identifier 10.1109/JPHOTOV.2015.2392945

2156-3381 © 2015 IEEE. Personal use is permitted, but republication/redistribution requires IEEE permission.
See http://www.ieee.org/publications_standards/publications/rights/index.html for more information.

IEEE Proof

order to complement the PL and Raman data, conductive-atomic force microscopy (c-AFM) measurements have been performed in order to study local resistance variations inside the LFCs.

It is worth to mention that the term LFC has been used since more than a decade to describe the firing of the predeposited aluminum through a dielectric layer. Despite the process used here is fundamentally different, its finality and application in solar cell devices is the same. For simplicity, we have maintained the term LFC to refer to our laser-processed locally doped regions.

II. Experimental Methods and Materials

Samples under study were based on 2.5 Ω·cm boron-doped float-zone (FZ) crystalline Si (c-Si) wafers with a thickness of 250 μm and (1 0 0) crystal orientation. c-Si wafers were passivated by a 25-nm-thick aluminum oxide (Al_2O_3) film which was grown by thermal atomic layer deposition. Laser fired spots were processed on the top of the Al_2O_3-passivated c-Si samples creating small apertures in the alumina layer and melting a small part of the underlying c-Si subsurface region. LFCs were processed by a 1064 nm Nd:YAG lamp-pumped laser working at 100 ns of pulse duration. Each contact is a consequence of six pulses at a repetition rate of 4 kHz. Three different LFCs processed with a laser power of 0.98, 1.1, and 1.43 W were studied, corresponding to pulse energies of 245, 275, and 357.5 μJ. The laser beam shows a Gaussian profile with a beam waist characterized by a radius of 70 μm at the focus plane where all the samples were processed. After laser processing and prior to carry out the measurements, samples were immersed in an HF 1% solution bath during 40 s (or until obtaining an hydrophobic silicon surface) in order to remove the Al_2O_3 layer. Additionally, three boron-doped FZ c-Si wafers with doping densities of 1×10^{15}, 5×10^{18}, and 1×10^{20} cm^{-3} were used in order to obtain reference Raman and PL spectra.

Micro-Raman and microphotoluminescence experiments were carried out with a WITEC alpha300. A diagram of the Witec equipment setup can be found in [8]. A diode-pumped laser with a wavelength of 532 nm was used as an excitation source resulting in a penetration depth of about 1 μm. Micro-Raman and micro-PL measurements were performed with a 100 × VIS (visible), NA (numerical aperture) = 0.9 and a 20 × IR (Infrared), NA = 0.45, respectively. The resulting beam spot size on the sample surface is in diameter below 1 and 2 μm for Raman and PL measurements, respectively. Raman scattering signal was recorded through a 300-mm imaging spectrometer equipped with both a 600 lines/mm and 1800 lines/mm grating, and a 1024 × 127 CCD (charge-coupled device) camera visible-optimized, whereas PL signal was collected through an additional 300-mm spectrometer composed of two gratings (150 and 300 lines/mm) and a 1024 × 1 pixel linear InGaAs photodiode array optimized for spectroscopy applications in the range 1–1.7 μm. It is worth to mention that the incoming laser power on the sample surface for the Raman measurements was kept below 3 mW. With our configuration, 3 mW was measured to be the pumping limit to keep the photo-generated carrier density below threshold and, therefore, to avoid Fano resonances induced by high injection conditions [15].

Local electrical measurements through the c-AFM technique were performed using a Digital Instruments Nanoscope IIIa Multimode AFM associated with the home-made conducting probe extension called "Resiscope" [9]. This extension allows us to apply a stable dc bias voltage (from −10 to +10 V) to the sample and to measure the resulting current flowing through the tip as the sample surface is scanned in contact mode, yielding a local resistance map covering resistance values in the range 10^2–10^{12} Ω. Current–Voltage (*I*–*V*) measurements are also permitted with this extension. Highly boron doped diamond-coated Si AFM cantilevers, with an intermediate spring constant of about 3 N/m, proved to be the most suitable AFM tips for making electrical measurements on LFCs. Due to the AFM tip radius (∼50 nm), c-AFM measurements offer a much greater lateral resolution. This latter depends on the electrical contact radius between the tip and the surface. In the particular case of flat surfaces, the electrical contact radius can be much smaller than AFM tip radius. The probed depth remains in the nanoscale range, but it is linked, among other parameters, to the applied voltage and the local electrical transport properties.

III. Results and Discussion

A. *Doping Characterization by Micro-Raman Spectroscopy*

Doping profiles in c-Si can be monitored by studying both the Full Width at Half Maximum (FWHM) [10] and the Fano resonance [11] of the first-order Si Raman peak. In particular, Fano resonances are evident in the Si Raman spectra at hole concentrations above 10^{18} cm^{-3} by a characteristic asymmetry in the first-order Si Raman line. This asymmetry results from the resonant interaction between discrete phonon states and a continuum of hole states [12], [13]. The Raman peak line shape can be described by the following expression [11]:

$$I(k) = I_0 \cdot \frac{[q + 2(k - k_{ph})/\Gamma]^2}{1 + [2(k - k_{ph})/\Gamma]^2} \quad (1)$$

where I_0 is a scaling factor, k_{ph} is the frequency associated to the Raman peak maximum, Γ corresponds to the FWHM, and q is the asymmetry parameter, which is correlated with the doping level of the sample being studied. The lower the q parameter, the higher the doping level. The first-order Si Raman peak can be also influenced by stress and/or by the material crystalline fraction. The former can be monitored by the peak frequency shift, whereas the latter is evidenced by a peak broadening from the c-Si to the amorphous-Si state.

Fig. 1 shows the optical microscope images (left-hand side) and the corresponding Raman peak width maps (right-hand side) of the three LFCs under study processed at 0.98 (a) and (b), 1.1 (c) and (d), and 1.43 W (e) and (f). Maps were obtained from the raw Raman peak width, not from the fitted Γ. The corresponding LFC diameters were 43.8, 54.5, and 74.2 μm, respectively. For ensuring a good observation of the obtained data, the microscope images and the Raman maps of the three contacts have been represented with a slightly different scale. In addition for clarity, the physical dimensions of the LFCs have been represented in Raman maps by a green dotted circle. As explained previously, the width of the first-order Raman peak

IEEE Proof

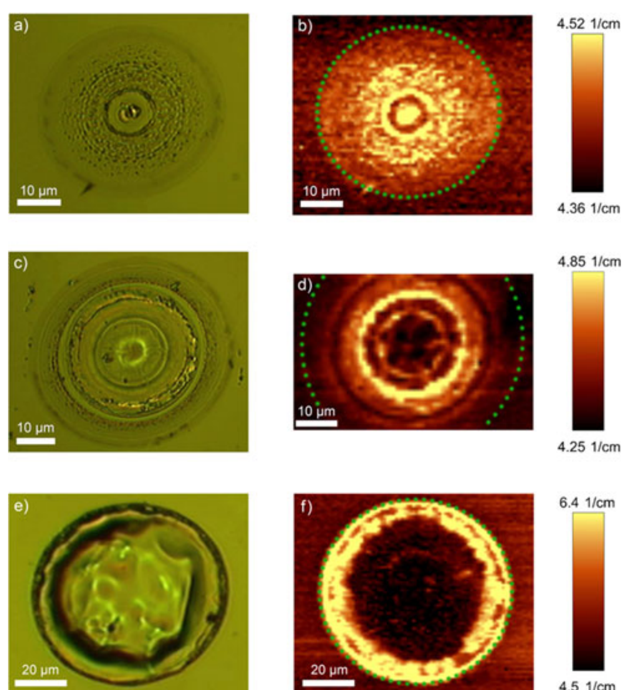

Fig. 1. Optical microscope images (left-hand side) and Raman peak width maps (right-hand side) of the three LFCs under study processed at 0.98 (a) and (b), 1.1 (c) and (d), and 1.43 W (e) and (f). Brighter zones in the Raman peak width maps correspond to zones with higher doping density.

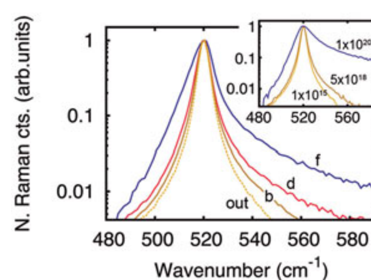

Fig. 2. Averaged Raman spectra corresponding to the brighter zones of maps b, d, and f of Fig. 1. For comparison, an averaged Raman spectra corresponding to an unprocessed surface area has been also represented (yellow dashed line). The inset shows the Raman spectra recorded from the three reference c-Si wafers with different doping level.

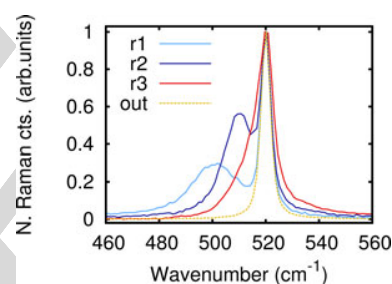

Fig. 3. Raman spectra obtained at specific points inside LFCs processed at 1.1 W (r1, r2) and 1.43 W (r3). In addition to the first-order Raman peak, a second peak characteristic of microcrystalline silicon sets in at lower wavenumbers. For comparison, a Raman peak related to an unprocessed area (outer region of LFCs) is also depicted.

can be used to monitor the doping level of the sample under study. Hence, the zones that evidence an increase of the Raman peak width in Fig. 1 (brighter zones) are qualitatively correlated with zones with a higher doping level. The LFC processed at 0.98 W evidences slightly higher levels of doping at the central part of the contact. In contrast, the contact processed at 1.1 W [see Fig. 1(d)] evidences a brighter concentric corona pointing out a wider Raman peak and consequently an increase of the doping level. Following the same trend, for the contact processed using the higher laser power [see Fig. 1(f)], the border of the contact is the area that evidences a higher level of doping. The different Raman maps illustrated in Fig. 1 demonstrate that the laser power plays an important role on the distribution of the highly doped regions inside the contacts. More precisely, it seems that for higher laser powers, the highly doped regions move toward the border of the contact. Two-dimensional depth profiling across LFCs (maps not shown for space limitations) revealed the same results. This fact corroborates that the features of Raman maps shown in Fig. 1 were not affected by variations in surface topography of LFCs.

The correlation between the Raman peak widening observed in Fig. 1 and the expected increase in the doping density is confirmed by data shown in Fig. 2. This figure shows the averaged Raman spectra corresponding to the zones with higher doping of images b, d, and f of Fig. 1. In particular, the averaged spectra were calculated from the yellow-colored areas of Raman maps. An averaged spectrum corresponding to an unprocessed area (outer region of LFC) is also shown (yellow dashed line). In order to facilitate the observation of Fano resonances, Raman spectra have been represented using a semilog scale. As it can be observed, the Fano resonance is clearly identified for all Raman spectra except for the one obtained out of the LFC, which shows a symmetric Raman line shape. This qualitatively confirms that the brighter zones in maps of Fig. 1 are correlated with areas with a higher doping level. The increase in doping is also greatly confirmed by the inset, where the Raman spectra recorded from three reference c-Si wafers with doping levels of 1×10^{15}, 5×10^{18}, and 1×10^{20} cm^{-3} clearly evidence the same trend concerning the Fano resonance. Another important feature observed in the main plot of Fig. 2 is that the LFCs processed with a higher laser power have associated a higher Fano asymmetry. Hence, the use of higher laser powers results in LFCs with higher doping densities.

In order to get further important information about the LFCs formation, we depict in Fig. 3 the Raman spectra recorded at three specific points (r1, r2, and r3) inside two LFCs processed at 1.1 W (r1, r2) and 1.43 W (r3) (contact images and point positions not shown). A fourth Raman spectrum corresponding to a nonprocessed surface area is also represented as a reference. As it can be observed, in addition to the first-order c-Si Raman line positioned at 520.9 cm^{-1}, new Raman bands can be identified at lower wavenumbers in the range between 500 and 515 cm^{-1}. These latter bands are commonly assigned to microcrystalline silicon [16], [17]. Indeed, the Raman

IEEE Proof

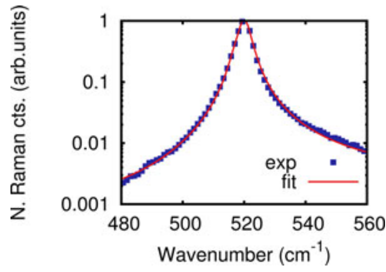

Fig. 4. Fitting using (2) of the Raman spectrum corresponding to the highly-doped region of the LFC processed at 1.1 W. Fit gave a q parameter of 59 which is correlated to a doping level of about 5.8×10^{18} cm^{-3}.

TABLE I
q ASYMMETRY PARAMETER OBTAINED FROM THE FITTING OF (2) TO THE AVERAGED RAMAN SPECTRA RELATED TO THE HIGHLY DOPED REGIONS OF THE THREE LFCS UNDER STUDY.

power (W)	q (arb.units)	doping ref. [10] ($\times10^{18}$ cm^{-3})	doping ref. [11] ($\times10^{18}$ cm^{-3})
0.98	90 ±7	3.13 – 3.83	1.17 – 2.35
1.10	61 ± 4	5.19 – 6.06	4.58 – 6.03
1.43	16 ± 2	21.49 – 27.93	42.19 – 50.17

The corresponding doping densities were calculated using the calibration tables reported in [10] and [11].

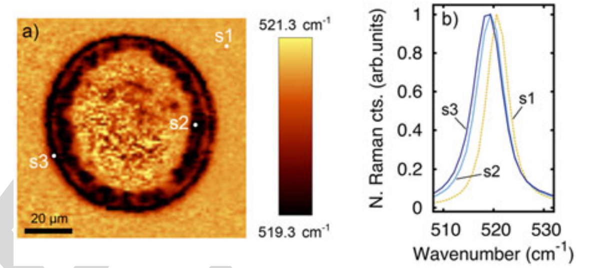

Fig. 5. (a) Raman spectra center of mass map of a LFC processed at 1.43 W. (b) Specific Raman spectra associated with points s1, s2, and s3 are also plotted.

spectra of microcrystalline-Si are currently decomposed into three bands: crystalline (~520 cm^{-1}), intermediate band (500–515 cm^{-1}, usually interpreted as a signature of the grain boundaries or small crystallites grain size <10 nm), and amorphous (480 cm^{-1}). The following decomposition is used to quantify the crystalline fraction [18]. The observation of these new Raman bands at specific points inside the LFCs suggests that molten Si material fraction solidifies in a structure involving crystallites, grain boundaries, and an amorphous phase, at least in specific zones inside the contacts. However, the crystalline fraction in these zones reveals to be high indicating a negligible amorphous component.

The contribution of microcrystalline-Si components to the obtained Raman spectra is further confirmed by the fact that all Raman spectra recorded inside the LFCs could be significantly better fitted using a rewriting of (1) that considers a second Lorentzian function related to the contribution of the microcrystalline Si formation. In fact, the expression that has been used to fit the Raman data is the following:

$$I(k) = I_0 \cdot \frac{[q + 2(k - k_{ph})/\Gamma]^2}{1 + [2(k - k_{ph})/\Gamma]^2} + \frac{A}{1 + [2(k - k_m)/\Gamma_m]^2} \quad (2)$$

where A corresponds to the intensity, k_m is the frequency of the peak maximum, and Γ_m is the peak width of the Raman band related to the microcrystalline-like component. It is worth to mention that the position of the second Lorentzian function was limited to values between 505 and 517 cm^{-1}. As observed in Fig. 4 for a LFC processed at 1.1 W, the fit using (2) shows very good adjustment paving the way to obtain a reliable quantification about the doping level inside the LFCs.

Table I shows the q asymmetry parameters resulting from the best fit of (2) to the Raman spectra related to the highly doped regions of the three LFCs under study. Data were calculated from at least two LFCs for each one of the three values of laser power. The obtained q parameters clearly illustrate that the higher the laser power, the higher the doping density. According to the calibration tables reported in [10] and [11], we have obtained maximum doping levels in the range of 1.17–3.83$\times10^{18}$, 4.58–6.06$\times10^{18}$, and 2.15–5.02$\times10^{19}$ cm^{-3} for the LFCs processed at 0.98, 1.1, and 1.43 W, respectively. It is important to remark that the intensity of the second Lorentzian peak related to the multicrystalline component was observed to increase with higher laser powers. This suggests that the use of higher laser powers decreases the crystalline fraction of the solidified Si volume.

Fig. 5(a) shows the Raman spectra center of mass map of a LFC processed at 1.43 W. The Raman spectra of the selected points (s1, s2, and s3) are represented in Fig. 5(b). The center of mass was calculated considering a frequency range between 480 and 560 cm^{-1}; thus, as confirmed by Raman spectra of Fig. 5(b), it could be qualitatively correlated with the frequency shift of the first-order Si Raman peak. The first-order Raman line of s1, s2, and s3 Raman spectra is centered at 520.8, 519.3, and 518.7 cm^{-1}, respectively. Notice that the center of mass values represented by the color scale bar of Fig. 5(a) are shifted toward higher frequencies respect the Raman peak position values mentioned previously. This is induced by the contribution of the Fano resonance which moves de center of mass toward higher energies respect the peak maximum. As it can be seen, the Raman peak position suffers a red shift of about 2 cm^{-1} at the border of the contact. Interestingly, areas of the contact that show such a red shift exactly match with areas of the 1.43 W LFC that evidence higher levels of doping [see Fig. 1(f)]. It has been reported, that Raman spectra obtained from samples with doping levels above 5×10^{18} cm^{-3} not only exhibit the so-called Fano resonance, but also show a red shift in the Raman peak maximum [19]. The expected theoretical peak shift induced by an increase in doping satisfies:

$$k = k_0 + \frac{\Delta\Gamma}{2\,q} \quad (3)$$

IEEE Proof

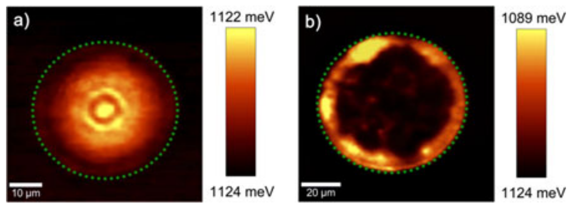

Fig. 6. PL center of mass maps of LFCs processed at (a) 0.98 W and (b) 1.43 W. The green dotted circles delimit the physical dimensions of the LFCs.

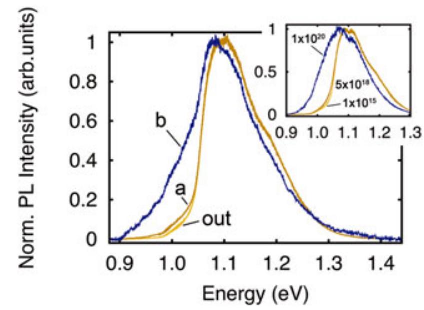

Fig. 7. Averaged PL spectra corresponding to the highly doped regions (yellow-colored regions) of PL center of mass maps a (0.98 W) and b (1.43 W) illustrated in Fig. 6. Additionally, a PL spectra recorded out of the processed LFC regions is also represented. The inset plot shows the PL spectra corresponding to three reference c-Si wafers with different doping level.

where k_0 is the peak position of the bulk un-doped and stress free c-Si and $\Delta\Gamma$ is the change in the Raman peak width due to doping. The expected theoretical peak shifts resulting from (3) for a q parameter of 16 (see Table I) takes values of about 0.5 cm^{-1}. These theoretical values are significantly lower than those observed in Fig. 5, i.e., about 2 cm^{-1}. This fact suggests that in addition to the red shift induced by an increase of the doping level, a second contribution in the Raman shift is also present. We correlate this second contribution with stress possibly induced by the laser process. LFCs processed at 0.98 and 1.1 W do not show any significant red shift in the first-order Raman peak maximum. Thus, the level of laser power used to process the LFCs probably plays an important role in the level of stress induced by the laser process.

B. Doping Characterization by Photoluminescence Spectroscopy

Band-to-band photoluminescence spectroscopy senses the radiative recombination between photo-generated electrons in the conduction band (CB) and the corresponding holes in the valence band (VB). As an increase in doping density induces a reduction of the energy gap between CB and VB, PL has been proven as a reliable tool for monitoring the band-gap shift in heavily doped c-Si [14]. In this sense, micro-PL spectroscopy is also capable to characterize the high doping levels expected inside the LFCs. In fact, micro-PL has been applied to characterize the doping density in laser-induced highly doped regions cross sections [7]. In our study, we study the position and line shape of the PL emission line by monitoring the center of mass of the PL spectra recorded inside the LFCs.

Fig. 6 shows the PL center of mass maps corresponding to the LFCs processed at 0.98 (a) and 1.43 W (b). The averaged PL spectra obtained from the brighter zones of the PL maps are illustrated in Fig. 7. As it can be seen, the shift of the PL spectra center of mass revealed by the color scale bars of Fig. 6 is linked to an increase of the PL intensity at lower energies. In particular, the PL spectrum related to the 0.98 W LFC evidences a slight increase of the left PL spectrum shoulder, whereas the PL spectrum related to the 1.43 W LFC shows a significantly higher increase of the left PL spectrum shoulder plus a blue shift in the PL emission maximum. We correlate this shift of the PL line with a Si band-gap renormalization induced by a strong increase of doping in the measured material volume. The increase in the doping density is further confirmed by the inset of Fig. 7 which illustrates the PL spectra recorded from c-Si wafers with doping levels of 1×10^{15}, 5×10^{18}, and 1×10^{20} cm^{-3}. As it can be seen, the inset and the main plot show the same trend. For all these reasons, we confirm that the brighter zones of the PL maps of Fig. 6 have associated a higher doping level. Interestingly, the two represented PL maps greatly correlate with the homologous Raman width maps of Fig. 1, demonstrating the successful application of micro-Raman and micro-PL techniques for studying doping-density variations above 1×10^{18} cm^{-3} with submicron resolution.

C. Laser-Fired Contact Characterization by Conductive-Atomic Force Microscopy

Finally, the study of LFCs was completed by their characterization by means of c-AFM measurements. The aim of these studies is to analyze if the laser-processed material volume shows preferential conductive zones, and if that is the case, to study their correlation with the highly doped regions deduced from Raman and PL data. C-AFM measurements have been divided in two groups. First, we have performed electrical maps of complete LFCs with the intention to qualitatively evidence differences in terms of electrical conductivity. In addition to the electrical maps, *I–V* measurements were also performed. These measurements were done in static mode at various locations onto the LFCs. In order to minimize the well-known light scattering effects from the AFM laser, which can induce local photoconductivity [20], the laser was turned-off for a brief moment before the *I–V* acquisition.

Representative c-AFM results obtained from a LFC processed at 1.43 W are shown in Fig. 8(a). The upper part of the image shows the topography map, whereas the lower part of the panel corresponds to the local resistance map recorded while applying a voltage of +2 V. In the latter, the darker zones indicate the areas with a low local resistance, i.e., high conductivity. In particular, the border of the contact shows the highest electrical conductivities which decrease as you move to the center of the contact. The highest local resistance was evidenced in outer region of the LFC (region that has not been processed). C-AFM data is in great agreement with Raman and PL data showed in the first part of the work, where highly doped regions of the contact processed at 1.43 W were detected at the border of the contact.

IEEE Proof

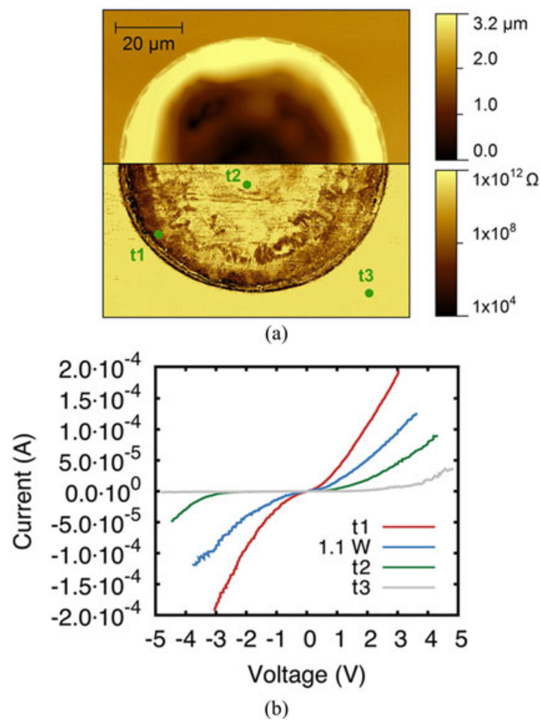

Fig. 8. (a) Topography (upper half) and local resistance (lower half) maps of a LFC processed at 1.43 W. (b) *I–V* characteristics of the selected points t1, t2, and t3 are represented. Additionally, an *I–V* curve (in blue) corresponding to a highly conductive area in a LFC processed at 1.1 W is also shown.

The *I–V* curves corresponding to the three points (t1, t2, and t3) depicted in the local resistance map of Fig. 8(a) are represented in Fig. 8(b). The curves have been calculated from an average of at least 20 curves per point. As expected from the resistivity map, the curve recorded at point t1 is the one that shows a higher conductivity. Moreover, it also shows a good linearity evidencing an ohmic contact behavior between the diamond tip and the sample. In contrast, the *I–V* curve recorded at point t2 (central part of the contact) evidences lower conductivity than that obtained at point t1. In addition, t2 curve shows a rectifying behavior. This can be explained by a higher potential barrier between the diamond tip and the less doped Si region. Of course, this scenario is even more evident for the *I–V* curve measured on the unprocessed region (t3). The potential barrier between the diamond tip and the nonprocessed surface (with a related doping density of about 5×10^{15} cm^{-3}) enlarges, creating a Schottky-like contact. In order to strengthen the consistency of the measurements, another *I–V* curve obtained onto the highly doped region of a contact processed at 1.1 W is also shown. As it was expected, the *I–V* curve shows a lower conductivity than the curve related to the LFC processed at 1.43 W. Again, the symmetry of the curve confirms the ohmic-like behavior of the contact between the tip and the highly doped sample region.

IV. Conclusion

In summary, the doping profiles in LFCs processed between 0.98 and 1.43 W in Al_2O_3-passivated p-type c-Si wafers have been studied. The laser power used to process the LFCs has been found to play an important role in the distribution of the highly doped regions. At powers around 1 W, the highly doped regions that reach doping levels of 2×10^{18} cm^{-3} are preferentially located at the center of the LFCs. In contrast, for higher laser power values, the level of doping increases (levels of around 3×10^{19} cm^{-3} has been observed for contacts processed at 1.43 W), and the location of the highly doped regions moves toward the border of the contacts. The high spatial resolution associated with our micro-Raman measurements has allowed to obtain consistent doping density values. Hence, micro-Raman is preferably the more appropriate tool to quantify doping levels with submicron resolution. We consider an important result the observation of microcrystalline-like features in the Raman spectra recorded at specific points inside the LFCs, which suggests that the locally molten Si fraction solidifies in microcrystalline manner.

Highly doped regions revealed by Raman measurements have been further confirmed by micro-PL spectroscopy. Regions with a higher doping density evidenced a blue shift of the PL emission line, which we correlate with the Si band-gap renormalization induced by the strong increase in doping. Despite the sample volume measured by micro-PL is typically higher, and therefore, the spatial resolution is lower, micro-PL measurements have also shown a good sensitivity to doping variations. The high injection conditions and the subsequent reduction of the photo-generated carriers diffusion length [8] could favor to reduce the spatial resolution of micro-PL measurements.

Finally, Raman and PL data have been further confirmed by local *I–V* curves recorded through conductive-AFM. *I–V* characteristics obtained on highly doped areas featured an ohmic-like behavior, whereas *I–V* curves recorded at regions nonprocessed by laser, i.e., regions with lower doping level, revealed a Schottky-like behavior.

Acknowledgment

The authors would like to thank C. Voz and P. Ortega for fruitful discussions.

References

[1] E. Schneiderlochner, R. Preu, R. Ldemann, and S. W. Glunz, “Laser-fired rear contacts for crystalline silicon solar cells,” *Prog. Photovoltaic, Res. Appl.*, vol. 10, pp. 29–34, 2002.

[2] D. Kray and S. Glunz, “Investigation of laser-fired rear-side recombination properties using an analytical model,” *Prog. Photovoltaic, Res. Appl.*, vol. 14, pp. 195–201, 2006.

[3] P. Ortega, A. Orpella, I. Martin, M. Colina, G. Lopez, C. Voz, M. I. Sanchez, C. Molpeceres, and R. Alcubilla, “Laser-fired contact optimization in c-Si solar cells,” *Prog. Photovoltaic, Res. Appl.*, vol. 20, pp. 173–180, 2012.

[4] M. Moors, K. Baert, T. Caremans, F. Duerinckx, A. Cacciato, and J. Szlufcik, “Industrial PERL-type solar cells exceeding 19% with screen-printed contacts and homogeneous emitter,” *Sol. Energy Mat. Sol. C.*, vol. 106, pp. 84–88, 2012.

[5] S. Glunz, A. Grobe, M. Hermle, M. Hofmann, S. Janz, T. Roth, O. Schultz, M. Vetter, I. Martín, R. Ferre, S. Bermejo, W. Wolke, W. Warta, and R. Willeke. “Comparison of different dielectric passivation layers for application in industrially feasible high-efficiency crystalline silicon solar cells,” *Proc. 20th Eur. Photovoltaic Sol. Energy Conf.*, 2005, pp. 572–577.

[6] P. Ortega, I. Martín, G. Lopez, M. Colina, A. Orpella, C. Voz, and R. Alcubilla, “P-type c-Si solar cells based on rear side laser processing of Al2O3/SiCx stacks,” *Sol. Energy Mat. Sol. C.*, vol. 106, pp. 80–83, 2012.

IEEE Proof

[7] P. Gundel, D. Suwito, U. Jger, F. D. Heinz, W. Warta, and M. C. Schubert, "Comprehensive microscopic analysis of laser-induced high doping regions in silicon," *IEEE Trans. Electron Devices*, vol. 58, no. 9, pp. 2874–2877, Sep. 2011.

[8] P. Gundel, F. D. Heinz, M. C. Schubert, J. A. Giesecke, and W. Warta, "Quantitative carrier lifetime measurement with micron resolution," *J. Appl. Phys.*, vol. 108, pp. 033705-1–033705-7 2010.

[9] F. Houzé, R. Meyer, O. Schneegans, and L. Boyer, "Imaging the local electrical properties of metal surfaces by atomic force microscopy with conducting probes," *Appl. Phys. Lett.*, vol. 69, pp. 1975–1977, 1996.

[10] T. Kunz, M. Hessmann, S. Seren, B. Meidel, B. Terheiden, and C. Brabec, "Dopant mapping in highly p-doped silicon by micro-Raman spectroscopy at various injection levels," *J. Appl. Phys.*, vol. 113, p. 023514, 2013.

Q1 [11] M. Becker, U. Gosele, A. Hofmann, and S. Christiansen, "Highly p-doped regions in silicon solar cells quantitatively analyzed by small angle beveling and micro-Raman spectroscopy," *J. Appl. Phys.*, vol. 106, p. 074515, 2009.

[12] U. Fano, "Effects of configuration interaction on intensities and phase shifts," *Phys. Rev.*, vol. 124, pp. 1866–1878, 1961.

[13] F. Cerdeira, T. Fjeldly, and M. Cardona, "Effect of free carriers on zone-center vibrational modes in heavily doped p-type Si. II. Optical modes," *Phys. Rev. B*, vol. 8, pp. 4734–4745, 1973.

[14] J. Wagner, "Band-gap narrowing in heavily doped silicon at 20 and 300 K studied by photoluminescence," *Phys. Rev. B*, vol. 32, pp. 1323–1325, 1985.

[15] V. Magidson and R. Beserman, "Fano-type interference in the Raman spectrum of photoexcited Si," *Phys. Rev. B*, vol. 66, pp. 1952061–1952066, 2002.

[16] S. Veprek, F.-A. Sarott, and Z. Iqbal, "Effect of grain boundaries on the Raman spectra, optical absorption, and elastic light scattering in nanometer-sized crystalline silicon," *Phys. Rev. B*, vol. 36, pp. 3344–3350, 1987.

[17] Z. Iqbal, S. Veprek, A. Webb, and P. Capezzuto, "Raman scattering from small particle size polycrystalline silicon," *Solid State Commun.*, vol. 37, pp. 993–996, 1981.

[18] T. Kaneko, K. Onisawa, M. Wakagi, Y. Kita, and T. Minemura, "Crystalline fraction of microcrystalline silicon films prepared by plasma-enhanced chemical vapor deposition using pulsed silane flow," *Jpn. J. Appl. Phys.*, vol. 32, p. 4907, 1993.

[19] R. Agaiby, M. Becker, S. Thapa, U. Urmoneit, A. Berger, A. Gawlik, G. Sarau, and S. Christiansen, "Stress and doping uniformity of laser crystallized amorphous silicon in thin film silicon solar cells," *J. Appl. Phys.*, vol. 107, p. 054312, 2010.

[20] M. Ledinský, A. Fejfar, A. Vetushka, J. Stuchlík, B. Rezek, and J. Kocka, "Local photoconductivity of microcrystalline silicon thin films measured by conductive atomic force microscopy," *Phys. Status Solidi RRL*, vol. 5, pp. 373–375, 2011.

Authors' photographs and biographies not available at the time of publication.

IEEE Proof

525

QUERIES

526 Q1. Author: Please provide the complete page range in Refs. [10], [11], [18], and [19].

IEEE Proof

Microscale Spatially Resolved Characterization of Highly Doped Regions in Laser-Fired Contacts for High-Efficiency Crystalline Si Solar Cells

A. Roigé, J. Alvarez, J.-P. Kleider, I. Martín, R. Alcubilla, and L. F. Vega

***Abstract*—Laser-fired contact (LFC) processes have emerged as a promising approach to create rear local electric contacts in p-type crystalline silicon solar cells. Despite this approach has been successfully applied in devices showing efficiencies above 20%, there is still a lack of knowledge about some specific features of LFCs at the submicron level. In this study, we used micro-Raman and microphotoluminescence (PL) spectroscopies to carry out a high-resolution spatially resolved characterization of LFCs processed in Al_2O_3-passivated c-Si wafers. Relevant information concerning features such as local doping distribution and crystalline fraction of the laser-processed region has been obtained. In particular, interesting qualitative and quantitative variations concerning the doping profile have been observed between LFCs processed at different laser powers. Finally, conductive-atomic force microscopy measurements have allowed to identify the existence of highly conductive zones inside the LFCs greatly correlated with highly doped regions revealed by Raman and PL data. This study gives a detailed insight about the LFCs characteristics at the submicron level and their possible influence on the performance of final devices.**

***Index Terms*—Crystalline silicon, laser-fired contacts (LFCs), microphotoluminescence spectroscopy, micro-Raman spectroscopy.**

I. Introduction

FROM an industrial point of view, one of the most interesting crystalline silicon (c-Si) solar cell technologies to obtain high-efficiency devices is the passivated emitter and rear cell concept. Recently, the industrial implementation of this cell type has been significantly simplified by using the so-called laser fired contact (LFC) approach for the creation of the back contacts of the cell [1], [2]. This method is based on firing the rear Al metallization layer by a laser beam in order to create electrical point contacts between the Al layer and the silicon substrate through the passivation layer.

A key feature for the good operation of LFCs is the formation of an Al-doped p+ region under the contacted surface area. This is achieved by the diffusion of Al atoms from the predeposited Al layer into the molten Si. This p+ region not only creates a local back-surface field that induces a relatively low recombination velocity below the contacts, but also ensures a low-contact resistance.

LFC approach can be applied by using any of the dielectric layers that have demonstrated excellent c-Si passivating properties such as silicon oxide (SiO_2) [3], silicon nitride (SiN_x) [4], amorphous-silicon carbide (a-SiC_x) [5], and most recently, aluminum oxide (Al_2O_3) [6]. In the case of using the latter passivating material, an interesting alternative to the conventional LFC process can be applied. In this case, the Al_2O_3 layer itself can be used as Al-dopant source for the formation of the p+ region, and hence, the LFC can be done directly onto the Al_2O_3/c-Si, instead of being done onto the Al/dielectric/c-Si stack. This approach enables a lower laser power operation in comparison with conventional LFC process where higher laser powers are needed to fire the aluminum through the dielectric layer. These type of LFC processes have been already used to fabricate solar cells showing efficiencies well above 20% [6].

Despite the evident success in the implementation of the LFC approach in real devices, there is still a lack of information about specific features of LFCs such as the doping profile of the p+ region, the level of induced-stress, and/or the structural properties of the laser-processed region. The most likely reason for that is the difficulty to find experimental techniques that match a high-lateral resolution (below 10 μm) and sensitivity to the parameters wanted to be studied. Recently, a study of LFC cross sections [7] have demonstrated that Raman and photoluminescence (PL) spectroscopies in microconfiguration are techniques that fulfill the mentioned requirements.

In this study, we have carried out high-resolution micro-Raman and micro-PL spectroscopy measurements on different LFCs processed in Al_2O_3-passivated c-Si samples. Thanks to the high lateral resolution down to 1 μm achieved in our experiments, we have been able to perform a detailed study of relevant LFC properties such as the doping profile, induced-stress, and crystallinity fraction, giving an important insight about the LFC formation. Three LFCs processed at different incident laser power have been studied in order to analyze the influence of the laser power on the studied features. Finally, in

Manuscript received October 29, 2014; revised December 20, 2014; accepted January 5, 2015. This work was supported by Carburos Metálicos/Air Products Group, the Generalitat of Catalonia (Project SGR2014-1582), and the Spanish Government (Project TEC2011-26329). This work was also supported in part by the project HERCULES that has received funding from the European Union's Seventh Programme for Research Technological Development and Demonstration under Grant Agreement 608498. The work of A. Roigé was supported through a TALENT fellowship from the Generalitat of Catalonia.

A. Roigé is with MATGAS Research Center, 08193 Bellaterra, Spain (e-mail: aroige@matgas.org).

J. Álvarez and J.-P. Kleider are with the LGEP-Supelec, 91192 Gif sur Yvette, France (e-mail: jose.alvarez@lgep.supelec.fr).

I. Martín and R. Alcubilla are with the Departament d'Enginyeria Electrònica, Universitat Politècnica de Catalunya, 08034 Barcelona, Spain (e-mail: isidro.martin@upc.edu; ramon.alcubilla@upc.edu).

L. F. Vega is with MATGAS Research Center, Carburos Metálicos-Air Products Group, 08009 Barcelona, Spain (e-mail: vegal@carburos.com).

Color versions of one or more of the figures in this paper are available online at http://ieeexplore.ieee.org.

Digital Object Identifier 10.1109/JPHOTOV.2015.2392945

2156-3381 © 2015 IEEE. Personal use is permitted, but republication/redistribution requires IEEE permission. See http://www.ieee.org/publications_standards/publications/rights/index.html for more information.

IEEE Proof

order to complement the PL and Raman data, conductive-atomic force microscopy (c-AFM) measurements have been performed in order to study local resistance variations inside the LFCs.

It is worth to mention that the term LFC has been used since more than a decade to describe the firing of the predeposited aluminum through a dielectric layer. Despite the process used here is fundamentally different, its finality and application in solar cell devices is the same. For simplicity, we have maintained the term LFC to refer to our laser-processed locally doped regions.

II. Experimental Methods and Materials

Samples under study were based on 2.5 Ω·cm boron-doped float-zone (FZ) crystalline Si (c-Si) wafers with a thickness of 250 μm and (1 0 0) crystal orientation. c-Si wafers were passivated by a 25-nm-thick aluminum oxide (Al_2O_3) film which was grown by thermal atomic layer deposition. Laser fired spots were processed on the top of the Al_2O_3-passivated c-Si samples creating small apertures in the alumina layer and melting a small part of the underlying c-Si subsurface region. LFCs were processed by a 1064 nm Nd:YAG lamp-pumped laser working at 100 ns of pulse duration. Each contact is a consequence of six pulses at a repetition rate of 4 kHz. Three different LFCs processed with a laser power of 0.98, 1.1, and 1.43 W were studied, corresponding to pulse energies of 245, 275, and 357.5 μJ. The laser beam shows a Gaussian profile with a beam waist characterized by a radius of 70 μm at the focus plane where all the samples were processed. After laser processing and prior to carry out the measurements, samples were immersed in an HF 1% solution bath during 40 s (or until obtaining an hydrophobic silicon surface) in order to remove the Al_2O_3 layer. Additionally, three boron-doped FZ c-Si wafers with doping densities of 1×10^{15}, 5×10^{18}, and 1×10^{20} cm^{-3} were used in order to obtain reference Raman and PL spectra.

Micro-Raman and microphotoluminescence experiments were carried out with a WITEC alpha300. A diagram of the Witec equipment setup can be found in [8]. A diode-pumped laser with a wavelength of 532 nm was used as an excitation source resulting in a penetration depth of about 1 μm. Micro-Raman and micro-PL measurements were performed with a 100 × VIS (visible), NA (numerical aperture) = 0.9 and a 20 × IR (Infrared), NA = 0.45, respectively. The resulting beam spot size on the sample surface is in diameter below 1 and 2 μm for Raman and PL measurements, respectively. Raman scattering signal was recorded through a 300-mm imaging spectrometer equipped with both a 600 lines/mm and 1800 lines/mm grating, and a 1024 × 127 CCD (charge-coupled device) camera visible-optimized, whereas PL signal was collected through an additional 300-mm spectrometer composed of two gratings (150 and 300 lines/mm) and a 1024 × 1 pixel linear InGaAs photodiode array optimized for spectroscopy applications in the range 1–1.7 μm. It is worth to mention that the incoming laser power on the sample surface for the Raman measurements was kept below 3 mW. With our configuration, 3 mW was measured to be the pumping limit to keep the photo-generated carrier density below threshold and, therefore, to avoid Fano resonances induced by high injection conditions [15].

Local electrical measurements through the c-AFM technique were performed using a Digital Instruments Nanoscope IIIa Multimode AFM associated with the home-made conducting probe extension called "Resiscope" [9]. This extension allows us to apply a stable dc bias voltage (from −10 to +10 V) to the sample and to measure the resulting current flowing through the tip as the sample surface is scanned in contact mode, yielding a local resistance map covering resistance values in the range 10^2–10^{12} Ω. Current–Voltage (*I–V*) measurements are also permitted with this extension. Highly boron doped diamond-coated Si AFM cantilevers, with an intermediate spring constant of about 3 N/m, proved to be the most suitable AFM tips for making electrical measurements on LFCs. Due to the AFM tip radius (∼50 nm), c-AFM measurements offer a much greater lateral resolution. This latter depends on the electrical contact radius between the tip and the surface. In the particular case of flat surfaces, the electrical contact radius can be much smaller than AFM tip radius. The probed depth remains in the nanoscale range, but it is linked, among other parameters, to the applied voltage and the local electrical transport properties.

III. Results and Discussion

A. Doping Characterization by Micro-Raman Spectroscopy

Doping profiles in c-Si can be monitored by studying both the Full Width at Half Maximum (FWHM) [10] and the Fano resonance [11] of the first-order Si Raman peak. In particular, Fano resonances are evident in the Si Raman spectra at hole concentrations above 10^{18} cm^{-3} by a characteristic asymmetry in the first-order Si Raman line. This asymmetry results from the resonant interaction between discrete phonon states and a continuum of hole states [12], [13]. The Raman peak line shape can be described by the following expression [11]:

$$I(k) = I_0 \cdot \frac{[q + 2(k - k_{ph})/\Gamma]^2}{1 + [2(k - k_{ph})/\Gamma]^2} \quad (1)$$

where I_0 is a scaling factor, k_{ph} is the frequency associated to the Raman peak maximum, Γ corresponds to the FWHM, and q is the asymmetry parameter, which is correlated with the doping level of the sample being studied. The lower the q parameter, the higher the doping level. The first-order Si Raman peak can be also influenced by stress and/or by the material crystalline fraction. The former can be monitored by the peak frequency shift, whereas the latter is evidenced by a peak broadening from the c-Si to the amorphous-Si state.

Fig. 1 shows the optical microscope images (left-hand side) and the corresponding Raman peak width maps (right-hand side) of the three LFCs under study processed at 0.98 (a) and (b), 1.1 (c) and (d), and 1.43 W (e) and (f). Maps were obtained from the raw Raman peak width, not from the fitted Γ. The corresponding LFC diameters were 43.8, 54.5, and 74.2 μm, respectively. For ensuring a good observation of the obtained data, the microscope images and the Raman maps of the three contacts have been represented with a slightly different scale. In addition for clarity, the physical dimensions of the LFCs have been represented in Raman maps by a green dotted circle. As explained previously, the width of the first-order Raman peak

IEEE Proof

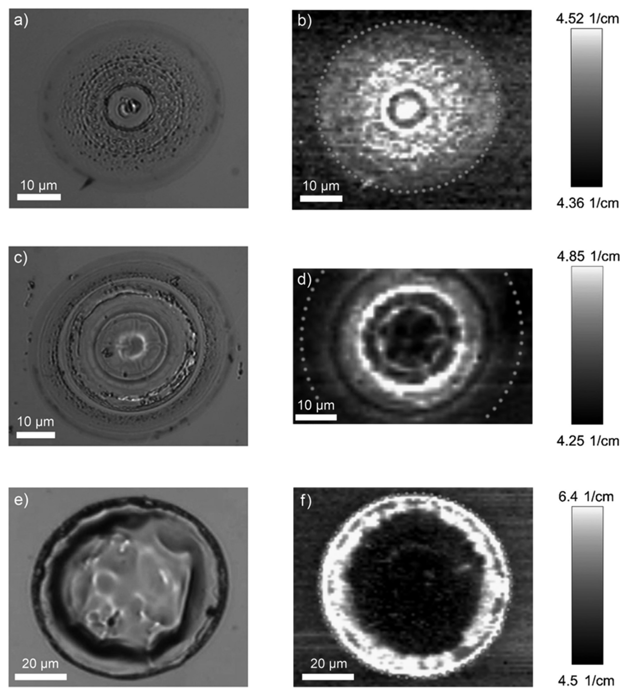

Fig. 1. Optical microscope images (left-hand side) and Raman peak width maps (right-hand side) of the three LFCs under study processed at 0.98 (a) and (b), 1.1 (c) and (d), and 1.43 W (e) and (f). Brighter zones in the Raman peak width maps correspond to zones with higher doping density.

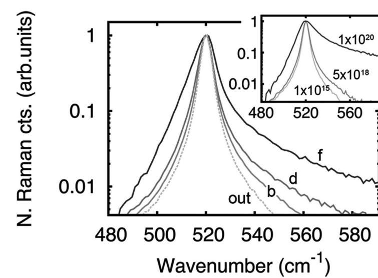

Fig. 2. Averaged Raman spectra corresponding to the brighter zones of maps b, d, and f of Fig. 1. For comparison, an averaged Raman spectra corresponding to an unprocessed surface area has been also represented (yellow dashed line). The inset shows the Raman spectra recorded from the three reference c-Si wafers with different doping level.

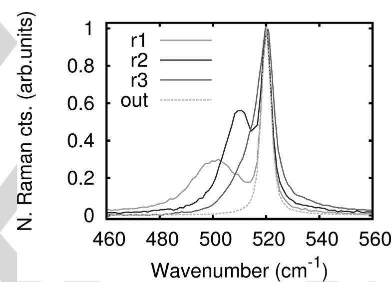

Fig. 3. Raman spectra obtained at specific points inside LFCs processed at 1.1 W (r1, r2) and 1.43 W (r3). In addition to the first-order Raman peak, a second peak characteristic of microcrystalline silicon sets in at lower wavenumbers. For comparison, a Raman peak related to an unprocessed area (outer region of LFCs) is also depicted.

can be used to monitor the doping level of the sample under study. Hence, the zones that evidence an increase of the Raman peak width in Fig. 1 (brighter zones) are qualitatively correlated with zones with a higher doping level. The LFC processed at 0.98 W evidences slightly higher levels of doping at the central part of the contact. In contrast, the contact processed at 1.1 W [see Fig. 1(d)] evidences a brighter concentric corona pointing out a wider Raman peak and consequently an increase of the doping level. Following the same trend, for the contact processed using the higher laser power [see Fig. 1(f)], the border of the contact is the area that evidences a higher level of doping. The different Raman maps illustrated in Fig. 1 demonstrate that the laser power plays an important role on the distribution of the highly doped regions inside the contacts. More precisely, it seems that for higher laser powers, the highly doped regions move toward the border of the contact. Two-dimensional depth profiling across LFCs (maps not shown for space limitations) revealed the same results. This fact corroborates that the features of Raman maps shown in Fig. 1 were not affected by variations in surface topography of LFCs.

The correlation between the Raman peak widening observed in Fig. 1 and the expected increase in the doping density is confirmed by data shown in Fig. 2. This figure shows the averaged Raman spectra corresponding to the zones with higher doping of images b, d, and f of Fig. 1. In particular, the averaged spectra were calculated from the yellow-colored areas of Raman maps. An averaged spectrum corresponding to an unprocessed area (outer region of LFC) is also shown (yellow dashed line). In order to facilitate the observation of Fano resonances, Raman spectra have been represented using a semilog scale. As it can be observed, the Fano resonance is clearly identified for all Raman spectra except for the one obtained out of the LFC, which shows a symmetric Raman line shape. This qualitatively confirms that the brighter zones in maps of Fig. 1 are correlated with areas with a higher doping level. The increase in doping is also greatly confirmed by the inset, where the Raman spectra recorded from three reference c-Si wafers with doping levels of 1×10^{15}, 5×10^{18}, and 1×10^{20} cm^{-3} clearly evidence the same trend concerning the Fano resonance. Another important feature observed in the main plot of Fig. 2 is that the LFCs processed with a higher laser power have associated a higher Fano asymmetry. Hence, the use of higher laser powers results in LFCs with higher doping densities.

In order to get further important information about the LFCs formation, we depict in Fig. 3 the Raman spectra recorded at three specific points (r1, r2, and r3) inside two LFCs processed at 1.1 W (r1, r2) and 1.43 W (r3) (contact images and point positions not shown). A fourth Raman spectrum corresponding to a nonprocessed surface area is also represented as a reference. As it can be observed, in addition to the first-order c-Si Raman line positioned at 520.9 cm^{-1}, new Raman bands can be identified at lower wavenumbers in the range between 500 and 515 cm^{-1}. These latter bands are commonly assigned to microcrystalline silicon [16], [17]. Indeed, the Raman

IEEE Proof

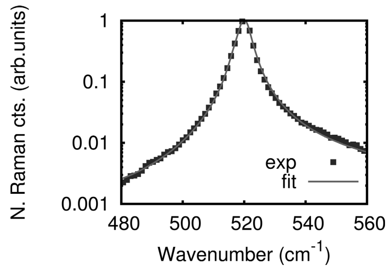

Fig. 4. Fitting using (2) of the Raman spectrum corresponding to the highly-doped region of the LFC processed at 1.1 W. Fit gave a q parameter of 59 which is correlated to a doping level of about 5.8×10^{18} cm^{-3}.

TABLE I
q ASYMMETRY PARAMETER OBTAINED FROM THE FITTING OF (2) TO THE AVERAGED RAMAN SPECTRA RELATED TO THE HIGHLY DOPED REGIONS OF THE THREE LFCS UNDER STUDY.

power (W)	q (arb.units)	doping ref. [10] ($\times10^{18}$ cm^{-3})	doping ref. [11] ($\times10^{18}$ cm^{-3})
0.98	90 ±7	3.13 – 3.83	1.17 – 2.35
1.10	61 ± 4	5.19 – 6.06	4.58 – 6.03
1.43	16 ± 2	21.49 – 27.93	42.19 – 50.17

The corresponding doping densities were calculated using the calibration tables reported in [10] and [11].

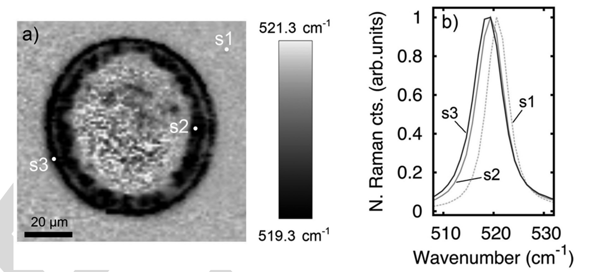

Fig. 5. (a) Raman spectra center of mass map of a LFC processed at 1.43 W. (b) Specific Raman spectra associated with points s1, s2, and s3 are also plotted.

spectra of microcrystalline-Si are currently decomposed into three bands: crystalline (~520 cm^{-1}), intermediate band (500–515 cm^{-1}, usually interpreted as a signature of the grain boundaries or small crystallites grain size <10 nm), and amorphous (480 cm^{-1}). The following decomposition is used to quantify the crystalline fraction [18]. The observation of these new Raman bands at specific points inside the LFCs suggests that molten Si material fraction solidifies in a structure involving crystallites, grain boundaries, and an amorphous phase, at least in specific zones inside the contacts. However, the crystalline fraction in these zones reveals to be high indicating a negligible amorphous component.

The contribution of microcrystalline-Si components to the obtained Raman spectra is further confirmed by the fact that all Raman spectra recorded inside the LFCs could be significantly better fitted using a rewriting of (1) that considers a second Lorentzian function related to the contribution of the microcrystalline Si formation. In fact, the expression that has been used to fit the Raman data is the following:

$$I(k) = I_0 \cdot \frac{[q + 2(k - k_{ph})/\Gamma]^2}{1 + [2(k - k_{ph})/\Gamma]^2} + \frac{A}{1 + [2(k - k_m)/\Gamma_m]^2} \quad (2)$$

where A corresponds to the intensity, k_m is the frequency of the peak maximum, and Γ_m is the peak width of the Raman band related to the microcrystalline-like component. It is worth to mention that the position of the second Lorentzian function was limited to values between 505 and 517 cm^{-1}. As observed in Fig. 4 for a LFC processed at 1.1 W, the fit using (2) shows very good adjustment paving the way to obtain a reliable quantification about the doping level inside the LFCs.

Table I shows the q asymmetry parameters resulting from the best fit of (2) to the Raman spectra related to the highly doped regions of the three LFCs under study. Data were calculated from at least two LFCs for each one of the three values of laser power. The obtained q parameters clearly illustrate that the higher the laser power, the higher the doping density. According to the calibration tables reported in [10] and [11], we have obtained maximum doping levels in the range of 1.17–3.83$\times10^{18}$, 4.58–6.06$\times10^{18}$, and 2.15–5.02$\times10^{19}$ cm^{-3} for the LFCs processed at 0.98, 1.1, and 1.43 W, respectively. It is important to remark that the intensity of the second Lorentzian peak related to the multicrystalline component was observed to increase with higher laser powers. This suggests that the use of higher laser powers decreases the crystalline fraction of the solidified Si volume.

Fig. 5(a) shows the Raman spectra center of mass map of a LFC processed at 1.43 W. The Raman spectra of the selected points (s1, s2, and s3) are represented in Fig. 5(b). The center of mass was calculated considering a frequency range between 480 and 560 cm^{-1}; thus, as confirmed by Raman spectra of Fig. 5(b), it could be qualitatively correlated with the frequency shift of the first-order Si Raman peak. The first-order Raman line of s1, s2, and s3 Raman spectra is centered at 520.8, 519.3, and 518.7 cm^{-1}, respectively. Notice that the center of mass values represented by the color scale bar of Fig. 5(a) are shifted toward higher frequencies respect the Raman peak position values mentioned previously. This is induced by the contribution of the Fano resonance which moves de center of mass toward higher energies respect the peak maximum. As it can be seen, the Raman peak position suffers a red shift of about 2 cm^{-1} at the border of the contact. Interestingly, areas of the contact that show such a red shift exactly match with areas of the 1.43 W LFC that evidence higher levels of doping [see Fig. 1(f)]. It has been reported, that Raman spectra obtained from samples with doping levels above 5×10^{18} cm^{-3} not only exhibit the so-called Fano resonance, but also show a red shift in the Raman peak maximum [19]. The expected theoretical peak shift induced by an increase in doping satisfies:

$$k = k_0 + \frac{\Delta\Gamma}{2\,q} \quad (3)$$

IEEE Proof

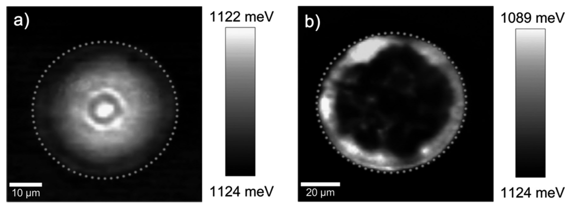

Fig. 6. PL center of mass maps of LFCs processed at (a) 0.98 W and (b) 1.43 W. The green dotted circles delimit the physical dimensions of the LFCs.

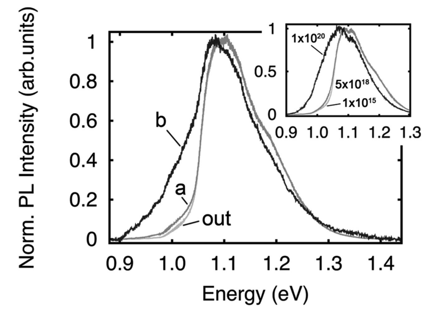

Fig. 7. Averaged PL spectra corresponding to the highly doped regions (yellow-colored regions) of PL center of mass maps a (0.98 W) and b (1.43 W) illustrated in Fig. 6. Additionally, a PL spectra recorded out of the processed LFC regions is also represented. The inset plot shows the PL spectra corresponding to three reference c-Si wafers with different doping level.

where k_0 is the peak position of the bulk un-doped and stress free c-Si and $\Delta\Gamma$ is the change in the Raman peak width due to doping. The expected theoretical peak shifts resulting from (3) for a q parameter of 16 (see Table I) takes values of about 0.5 cm^{-1}. These theoretical values are significantly lower than those observed in Fig. 5, i.e., about 2 cm^{-1}. This fact suggests that in addition to the red shift induced by an increase of the doping level, a second contribution in the Raman shift is also present. We correlate this second contribution with stress possibly induced by the laser process. LFCs processed at 0.98 and 1.1 W do not show any significant red shift in the first-order Raman peak maximum. Thus, the level of laser power used to process the LFCs probably plays an important role in the level of stress induced by the laser process.

B. Doping Characterization by Photoluminescence Spectroscopy

Band-to-band photoluminescence spectroscopy senses the radiative recombination between photo-generated electrons in the conduction band (CB) and the corresponding holes in the valence band (VB). As an increase in doping density induces a reduction of the energy gap between CB and VB, PL has been proven as a reliable tool for monitoring the band-gap shift in heavily doped c-Si [14]. In this sense, micro-PL spectroscopy is also capable to characterize the high doping levels expected inside the LFCs. In fact, micro-PL has been applied to characterize the doping density in laser-induced highly doped regions cross sections [7]. In our study, we study the position and line shape of the PL emission line by monitoring the center of mass of the PL spectra recorded inside the LFCs.

Fig. 6 shows the PL center of mass maps corresponding to the LFCs processed at 0.98 (a) and 1.43 W (b). The averaged PL spectra obtained from the brighter zones of the PL maps are illustrated in Fig. 7. As it can be seen, the shift of the PL spectra center of mass revealed by the color scale bars of Fig. 6 is linked to an increase of the PL intensity at lower energies. In particular, the PL spectrum related to the 0.98 W LFC evidences a slight increase of the left PL spectrum shoulder, whereas the PL spectrum related to the 1.43 W LFC shows a significantly higher increase of the left PL spectrum shoulder plus a blue shift in the PL emission maximum. We correlate this shift of the PL line with a Si band-gap renormalization induced by a strong increase of doping in the measured material volume. The increase in the doping density is further confirmed by the inset of Fig. 7 which illustrates the PL spectra recorded from c-Si wafers with doping levels of 1×10^{15}, 5×10^{18}, and 1×10^{20} cm^{-3}. As it can be seen, the inset and the main plot show the same trend. For all these reasons, we confirm that the brighter zones of the PL maps of Fig. 6 have associated a higher doping level. Interestingly, the two represented PL maps greatly correlate with the homologous Raman width maps of Fig. 1, demonstrating the successful application of micro-Raman and micro-PL techniques for studying doping-density variations above 1×10^{18} cm^{-3} with submicron resolution.

C. Laser-Fired Contact Characterization by Conductive-Atomic Force Microscopy

Finally, the study of LFCs was completed by their characterization by means of c-AFM measurements. The aim of these studies is to analyze if the laser-processed material volume shows preferential conductive zones, and if that is the case, to study their correlation with the highly doped regions deduced from Raman and PL data. C-AFM measurements have been divided in two groups. First, we have performed electrical maps of complete LFCs with the intention to qualitatively evidence differences in terms of electrical conductivity. In addition to the electrical maps, *I–V* measurements were also performed. These measurements were done in static mode at various locations onto the LFCs. In order to minimize the well-known light scattering effects from the AFM laser, which can induce local photoconductivity [20], the laser was turned-off for a brief moment before the *I–V* acquisition.

Representative c-AFM results obtained from a LFC processed at 1.43 W are shown in Fig. 8(a). The upper part of the image shows the topography map, whereas the lower part of the panel corresponds to the local resistance map recorded while applying a voltage of +2 V. In the latter, the darker zones indicate the areas with a low local resistance, i.e., high conductivity. In particular, the border of the contact shows the highest electrical conductivities which decrease as you move to the center of the contact. The highest local resistance was evidenced in outer region of the LFC (region that has not been processed). C-AFM data is in great agreement with Raman and PL data showed in the first part of the work, where highly doped regions of the contact processed at 1.43 W were detected at the border of the contact.

IEEE Proof

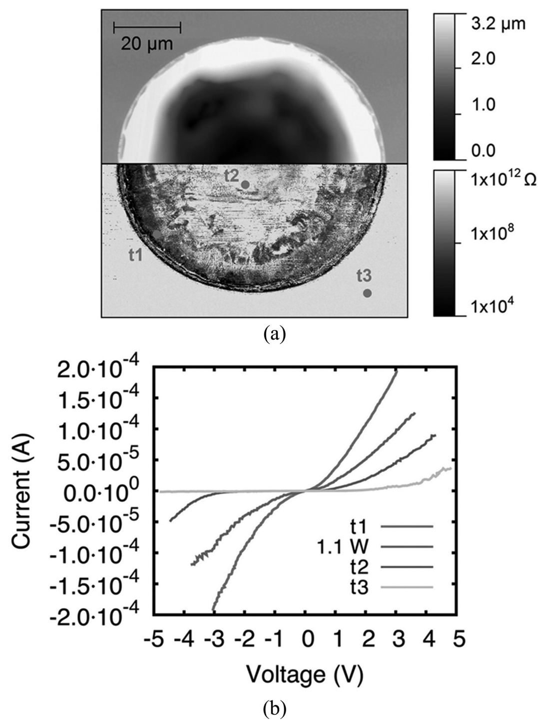

Fig. 8. (a) Topography (upper half) and local resistance (lower half) maps of a LFC processed at 1.43 W. (b) *I–V* characteristics of the selected points t1, t2, and t3 are represented. Additionally, an *I–V* curve (in blue) corresponding to a highly conductive area in a LFC processed at 1.1 W is also shown.

The *I–V* curves corresponding to the three points (t1, t2, and t3) depicted in the local resistance map of Fig. 8(a) are represented in Fig. 8(b). The curves have been calculated from an average of at least 20 curves per point. As expected from the resistivity map, the curve recorded at point t1 is the one that shows a higher conductivity. Moreover, it also shows a good linearity evidencing an ohmic contact behavior between the diamond tip and the sample. In contrast, the *I–V* curve recorded at point t2 (central part of the contact) evidences lower conductivity than that obtained at point t1. In addition, t2 curve shows a rectifying behavior. This can be explained by a higher potential barrier between the diamond tip and the less doped Si region. Of course, this scenario is even more evident for the *I–V* curve measured on the unprocessed region (t3). The potential barrier between the diamond tip and the nonprocessed surface (with a related doping density of about 5×10^{15} cm^{-3}) enlarges, creating a Schottky-like contact. In order to strengthen the consistency of the measurements, another *I–V* curve obtained onto the highly doped region of a contact processed at 1.1 W is also shown. As it was expected, the *I–V* curve shows a lower conductivity than the curve related to the LFC processed at 1.43 W. Again, the symmetry of the curve confirms the ohmic-like behavior of the contact between the tip and the highly doped sample region.

IV. Conclusion

In summary, the doping profiles in LFCs processed between 0.98 and 1.43 W in Al_2O_3-passivated p-type c-Si wafers have been studied. The laser power used to process the LFCs has been found to play an important role in the distribution of the highly doped regions. At powers around 1 W, the highly doped regions that reach doping levels of 2×10^{18} cm^{-3} are preferentially located at the center of the LFCs. In contrast, for higher laser power values, the level of doping increases (levels of around 3×10^{19} cm^{-3} has been observed for contacts processed at 1.43 W), and the location of the highly doped regions moves toward the border of the contacts. The high spatial resolution associated with our micro-Raman measurements has allowed to obtain consistent doping density values. Hence, micro-Raman is preferably the more appropriate tool to quantify doping levels with submicron resolution. We consider an important result the observation of microcrystalline-like features in the Raman spectra recorded at specific points inside the LFCs, which suggests that the locally molten Si fraction solidifies in microcrystalline manner.

Highly doped regions revealed by Raman measurements have been further confirmed by micro-PL spectroscopy. Regions with a higher doping density evidenced a blue shift of the PL emission line, which we correlate with the Si band-gap renormalization induced by the strong increase in doping. Despite the sample volume measured by micro-PL is typically higher, and therefore, the spatial resolution is lower, micro-PL measurements have also shown a good sensitivity to doping variations. The high injection conditions and the subsequent reduction of the photo-generated carriers diffusion length [8] could favor to reduce the spatial resolution of micro-PL measurements.

Finally, Raman and PL data have been further confirmed by local *I–V* curves recorded through conductive-AFM. *I–V* characteristics obtained on highly doped areas featured an ohmic-like behavior, whereas *I–V* curves recorded at regions nonprocessed by laser, i.e., regions with lower doping level, revealed a Schottky-like behavior.

Acknowledgment

The authors would like to thank C. Voz and P. Ortega for fruitful discussions.

References

[1] E. Schneiderlochner, R. Preu, R. Ldemann, and S. W. Glunz, “Laser-fired rear contacts for crystalline silicon solar cells,” *Prog. Photovoltaic, Res. Appl.*, vol. 10, pp. 29–34, 2002.

[2] D. Kray and S. Glunz, “Investigation of laser-fired rear-side recombination properties using an analytical model,” *Prog. Photovoltaic, Res. Appl.*, vol. 14, pp. 195–201, 2006.

[3] P. Ortega, A. Orpella, I. Martin, M. Colina, G. Lopez, C. Voz, M. I. Sanchez, C. Molpeceres, and R. Alcubilla, “Laser-fired contact optimization in c-Si solar cells,” *Prog. Photovoltaic, Res. Appl.*, vol. 20, pp. 173–180, 2012.

[4] M. Moors, K. Baert, T. Caremans, F. Duerinckx, A. Cacciato, and J. Szlufcik, “Industrial PERL-type solar cells exceeding 19% with screen-printed contacts and homogeneous emitter,” *Sol. Energy Mat. Sol. C.*, vol. 106, pp. 84–88, 2012.

[5] S. Glunz, A. Grobe, M. Hermle, M. Hofmann, S. Janz, T. Roth, O. Schultz, M. Vetter, I. Martín, R. Ferre, S. Bermejo, W. Wolke, W. Warta, and R. Willeke. “Comparison of different dielectric passivation layers for application in industrially feasible high-efficiency crystalline silicon solar cells,” *Proc. 20th Eur. Photovoltaic Sol. Energy Conf.*, 2005, pp. 572–577.

[6] P. Ortega, I. Martín, G. Lopez, M. Colina, A. Orpella, C. Voz, and R. Alcubilla, “P-type c-Si solar cells based on rear side laser processing of Al2O3/SiCx stacks,” *Sol. Energy Mat. Sol. C.*, vol. 106, pp. 80–83, 2012.

IEEE Proof

[7] P. Gundel, D. Suwito, U. Jger, F. D. Heinz, W. Warta, and M. C. Schubert, "Comprehensive microscopic analysis of laser-induced high doping regions in silicon," *IEEE Trans. Electron Devices*, vol. 58, no. 9, pp. 2874–2877, Sep. 2011.

[8] P. Gundel, F. D. Heinz, M. C. Schubert, J. A. Giesecke, and W. Warta, "Quantitative carrier lifetime measurement with micron resolution," *J. Appl. Phys.*, vol. 108, pp. 033705-1–033705-7 2010.

[9] F. Houzé, R. Meyer, O. Schneegans, and L. Boyer, "Imaging the local electrical properties of metal surfaces by atomic force microscopy with conducting probes," *Appl. Phys. Lett.*, vol. 69, pp. 1975–1977, 1996.

[10] T. Kunz, M. Hessmann, S. Seren, B. Meidel, B. Terheiden, and C. Brabec, "Dopant mapping in highly p-doped silicon by micro-Raman spectroscopy at various injection levels," *J. Appl. Phys.*, vol. 113, p. 023514, 2013.

Q1 [11] M. Becker, U. Gosele, A. Hofmann, and S. Christiansen, "Highly p-doped regions in silicon solar cells quantitatively analyzed by small angle beveling and micro-Raman spectroscopy," *J. Appl. Phys.*, vol. 106, p. 074515, 2009.

[12] U. Fano, "Effects of configuration interaction on intensities and phase shifts," *Phys. Rev.*, vol. 124, pp. 1866–1878, 1961.

[13] F. Cerdeira, T. Fjeldly, and M. Cardona, "Effect of free carriers on zone-center vibrational modes in heavily doped p-type Si. II. Optical modes," *Phys. Rev. B*, vol. 8, pp. 4734–4745, 1973.

[14] J. Wagner, "Band-gap narrowing in heavily doped silicon at 20 and 300 K studied by photoluminescence," *Phys. Rev. B*, vol. 32, pp. 1323–1325, 1985.

[15] V. Magidson and R. Beserman, "Fano-type interference in the Raman spectrum of photoexcited Si," *Phys. Rev. B*, vol. 66, pp. 1952061–1952066, 2002.

[16] S. Veprek, F.-A. Sarott, and Z. Iqbal, "Effect of grain boundaries on the Raman spectra, optical absorption, and elastic light scattering in nanometer-sized crystalline silicon," *Phys. Rev. B*, vol. 36, pp. 3344–3350, 1987.

[17] Z. Iqbal, S. Veprek, A. Webb, and P. Capezzuto, "Raman scattering from small particle size polycrystalline silicon," *Solid State Commun.*, vol. 37, pp. 993–996, 1981.

[18] T. Kaneko, K. Onisawa, M. Wakagi, Y. Kita, and T. Minemura, "Crystalline fraction of microcrystalline silicon films prepared by plasma-enhanced chemical vapor deposition using pulsed silane flow," *Jpn. J. Appl. Phys.*, vol. 32, p. 4907, 1993.

[19] R. Agaiby, M. Becker, S. Thapa, U. Urmoneit, A. Berger, A. Gawlik, G. Sarau, and S. Christiansen, "Stress and doping uniformity of laser crystallized amorphous silicon in thin film silicon solar cells," *J. Appl. Phys.*, vol. 107, p. 054312, 2010.

[20] M. Ledinský, A. Fejfar, A. Vetushka, J. Stuchlík, B. Rezek, and J. Kocka, "Local photoconductivity of microcrystalline silicon thin films measured by conductive atomic force microscopy," *Phys. Status Solidi RRL*, vol. 5, pp. 373–375, 2011.

Authors' photographs and biographies not available at the time of publication.

IEEE Proof

525

QUERIES

526 Q1. Author: Please provide the complete page range in Refs. [10], [11], [18], and [19].

IEEE Proof